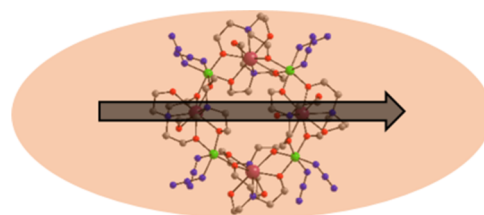


# Fe–Gd Ferromagnetic Cyclic Coordination Cluster [Fe<sup>III</sup><sub>4</sub>Gd<sup>III</sup><sub>4</sub>(teaH)<sub>8</sub>(N<sub>3</sub>)<sub>8</sub>(H<sub>2</sub>O)] with Magnetic Anisotropy—Theory and Experiment

Dirk Schray, Dennis Westerbeck, Jonas Braun, Yanhua Lan, Silvia Gómez-Coca, Wolfgang Wernsdorfer, Eliseo Ruiz, Christopher E. Anson, Jürgen Schnack,\* and Annie K. Powell\*

**ABSTRACT:** The synthesis, structural, and magnetic characterization of [Fe<sup>III</sup><sub>4</sub>Ln<sup>III</sup><sub>4</sub>(teaH)<sub>8</sub>(N<sub>3</sub>)<sub>8</sub>(H<sub>2</sub>O)] (Ln = Gd and Y) and the previously reported isostructural Dy analogue are discussed. The commonly held belief that both Fe<sup>III</sup> and Gd<sup>III</sup> can be regarded as isotropic ions is shown to be an oversimplification. This conclusion is derived from the magnetic data for the Y<sup>III</sup> analogue in terms of the zero-field splitting seen for Fe<sup>III</sup> and from the fact that the magnetic data for the new Gd<sup>III</sup> analogue can only be fit employing an additional anisotropy term for the Gd<sup>III</sup> ions. Furthermore, the Fe<sub>4</sub>Gd<sub>4</sub> ring shows slow relaxation of magnetization. Our analysis of the experimental magnetic data employs both density functional theory as well as the finite-temperature Lanczos method which finally enables us to provide an almost perfect fit of magnetocaloric properties.



Anisotropy of normally isotropic ions leads to slow relaxation

## INTRODUCTION

The concept of taking an Fe–Ln strand and cyclizing it has been previously described for a number of magnetically and optically interesting systems.<sup>1–6</sup> Cyclization of a certain strand length turns a 1D system into a 0D one<sup>7</sup> and allows for excitons to circulate in nanotoruses<sup>3</sup> and for toroidal moments to be stabilized.<sup>6</sup>

Here, we report the synthesis and structural and magnetic characterization of a ferrimagnetic Fe<sub>4</sub>Gd<sub>4</sub> ring. Contrary to popular belief both Fe<sup>III</sup> in its high spin state and Gd<sup>III</sup> should not be regarded as purely isotropic systems. In the case of high spin Fe<sup>III</sup>, significant axial and rhombic zero-field splitting (ZFS) parameters are found.<sup>8</sup> Single-ion |D| values are typically up to 0.2 cm<sup>-1</sup>, which partially explains the large number of Fe<sup>III</sup> single molecule magnet (SMM) systems.<sup>9–12</sup> Recently, single-ion Gd<sup>III</sup> systems have been reported to show slow relaxation of the magnetization which can only arise when there is some anisotropy induced by the crystal field,<sup>13–17</sup> with |D| typically up to ~0.1 cm<sup>-1</sup> for molecular systems.<sup>18–20</sup> However, higher values up to 0.17 cm<sup>-1</sup> have been found in solid-state systems.<sup>21</sup>

In the particular case of Fe<sub>10</sub>Gd<sub>10</sub>, it was found that significant next-nearest-neighbor antiferromagnetic interaction between the Fe<sup>III</sup> centers is a key parameter for stabilizing a system lying near to a quantum critical point as revealed by magnetocaloric effect (MCE) studies. The combination of these interactions and the ferromagnetic Fe–Gd coupling are balanced to be near the ideal ratio of 0.7 expected for a quantum critical system with these two ions, giving rise to a spin structure with a very high level of degeneracy, such that

the spin ground state of  $S = 120/2$  was close to a quantum critical point. However, such a large system can only be calculated making some simplifications in terms of the spin model as a result of the large Hilbert space. However, we found that no allowance needed to be made for any anisotropy in order to obtain a good fit to the experimental data.<sup>5</sup>

The Fe<sub>4</sub>Gd<sub>4</sub> system we report here is isostructural to the previously reported cyclic complex [Fe<sup>III</sup><sub>4</sub>Dy<sup>III</sup><sub>4</sub>(teaH)<sub>8</sub>(N<sub>3</sub>)<sub>8</sub>(H<sub>2</sub>O)] (**1-Dy**) in which Fe and Dy centers alternate around the ring.<sup>1</sup> The magnetic characterization of complex **1-Dy** showed ferromagnetic coupling between the Fe and Dy centers and SMM behavior. The isostructural gadolinium complex therefore seemed to be an ideal target to study the MCE in Fe<sup>III</sup>–Gd<sup>III</sup> complexes, as ferromagnetic coupling between Fe<sup>III</sup> and Gd<sup>III</sup> cations might also be expected. Fe<sub>4</sub>Gd<sub>4</sub> represents the smallest cyclic system in this family of Fe<sub>n</sub>Ln<sub>n</sub> compounds. In addition, this can be calculated using the real spin states of the metal ions without restrictions. This allows the Fe–Ln interaction to be investigated in a polynuclear system without this being swamped by much stronger direct Fe–Fe antiferromagnetic interactions.

The reaction of  $\text{FeCl}_3$ ,  $\text{GdCl}_3 \cdot 6\text{H}_2\text{O}$ , triethanolamine ( $\text{teaH}_3$ ), and  $\text{NaN}_3$  in a 2:1:3:2 molar ratio in  $\text{MeOH}/\text{MeCN}$  gave an orange solution from which yellow crystals of  $[\text{Fe}_4\text{Gd}_4(\text{teaH})_8(\text{N}_3)_8(\text{H}_2\text{O})] \cdot 4\text{MeCN} \cdot \text{H}_2\text{O}$  (**2-Gd**) appear after 3 days. The analogous reaction using  $\text{Y}(\text{NO}_3)_3 \cdot 6\text{H}_2\text{O}$  gave  $[\text{Fe}_4\text{Y}_4(\text{teaH})_8(\text{N}_3)_8] \cdot 5^{1/2}\text{MeCN}$  (**3-Y**).

The  $\text{Fe}_4\text{Gd}_4$  ring **2-Gd** is both isostructural and isomorphous to its  $\text{Fe}_4\text{Dy}_4$  analogue **1-Dy**<sup>1</sup> and so its structure will be described briefly here, emphasizing those features relevant to the present magnetic study. Two views of the molecular structure are shown in Figure 1.

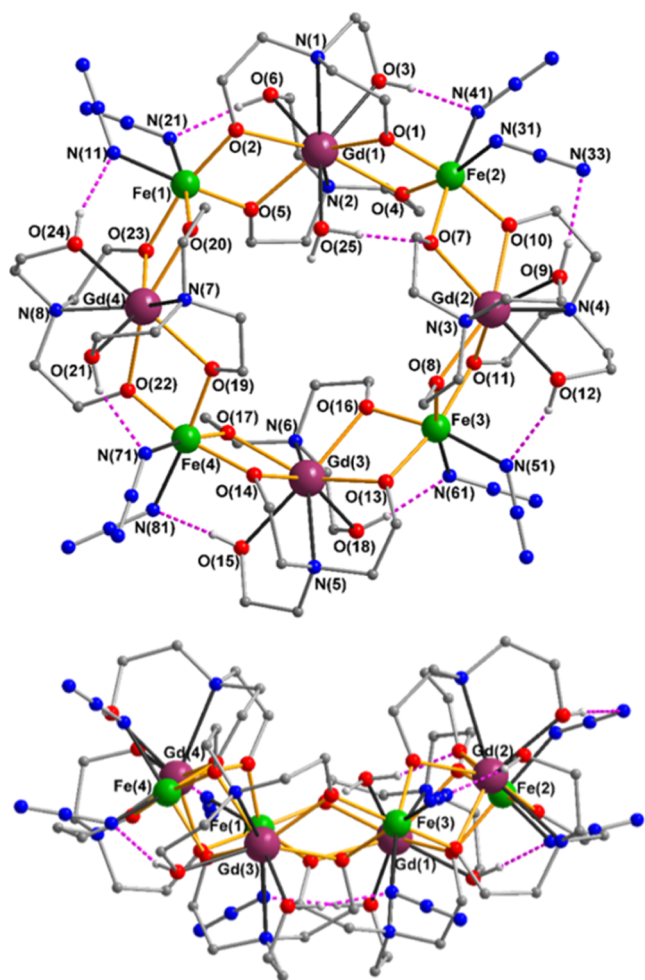


**Figure 1.** Two views of the molecular structure of  $[\text{Fe}_4\text{Gd}_4(\text{teaH})_8(\text{N}_3)_8(\text{H}_2\text{O})]$  (**2-Gd**).

The cyclic octanuclear structure of **2-Gd** is built up from alternating  $\{\text{Gd}^{\text{III}}(\text{teaH})_2\}^-$  and  $\{\text{Fe}^{\text{III}}(\text{N}_3)_2\}^+$  moieties. Each Gd center is chelated by two doubly deprotonated ( $\text{teaH}$ )<sup>2-</sup> ligands, of which the four deprotonated oxygens form pairwise alkoxy bridges to the adjacent Fe centers in the ring. Each of the still-protonated ethanol arms of the ligands coordinate to Gd in a non-bridging manner while also forming a hydrogen bond to an azide nitrogen on an adjacent Fe. Three of the Gd centers are eight-coordinate, while the nine-coordinate Gd(1) is ligated by an additional aqua ligand.

This distribution of doubly deprotonated triethanolamine ligands has also been observed in some other five- and six-membered Fe/Ln cyclic systems.<sup>7,22</sup> However, it differs from that found for the higher-nuclearity  $\text{Fe}_{10}\text{Gd}_{10}$  ring, in which

each metal ion is chelated by one methyltriethanolamine ligand, either doubly deprotonated around Gd or triply deprotonated on Fe, and the strong hydrogen bonding between doubly and triply deprotonated ligands then stabilizes the “cyclic standing wave” structure of the  $\text{Fe}_{10}\text{Gd}_{10}$  core. Nonetheless, the  $\text{Fe}_4\text{Gd}_4$  core in **2-Gd** still has  $\text{FeGd}$  moieties alternately above and below the mean plane of the ring, as can be seen in the side-on view in Figure 1, although the amplitude of the “standing wave” is now much less than that for the  $\text{Fe}_{10}\text{Gd}_{10}$  ring. A consequence of this is that the  $\text{Fe}-\text{Gd}-\text{Fe}$  angles in **2-Gd** ( $146.5$ ,  $130.1$ ,  $130.0$ ,  $133.8^\circ$ ) are much larger than that in the  $\text{Fe}_{10}\text{Gd}_{10}$  system ( $117.2-122.9^\circ$ ), which indicates that the next-nearest-neighbor  $\text{Fe}\cdots\text{Fe}$  magnetic interactions in **2-Gd** are likely to differ (probably being smaller) from those in the  $\text{Fe}_{10}\text{Gd}_{10}$ . By contrast, the  $\text{Fe}-\text{O}-\text{Gd}$  angles in **2-Gd**, which are all in the range  $105.4-108.9^\circ$ , are similar to those in the  $\text{Fe}_{10}\text{Gd}_{10}$  ( $103.6-108.2^\circ$ ), and the  $\text{Fe}-\text{O}$  and  $\text{Gd}-\text{O}$  bond lengths are also similar in the two molecules, such that the  $\text{Fe}-\text{Gd}$  interactions are likely to be comparable in the two rings.

## MAGNETIC PROPERTIES

We consider first the magnetic properties of  $\text{Fe}_4\text{Y}_4$  **3-Y**, in which the  $\text{Fe}^{\text{III}}$  ions alternate with diamagnetic  $\text{Y}^{\text{III}}$  ions around the ring, since this allows us to investigate the next-nearest-neighbor  $\text{Fe}-(\text{Y})-\text{Fe}$  magnetic interactions, and any anisotropy of the  $\text{Fe}^{\text{III}}$  cations. These properties can be carried over to the analysis of the  $\text{Fe}_4\text{Gd}_4$  ring (**2-Gd**).

At 300 K, the  $\chi_M T$  product for  $\text{Fe}_4\text{Y}_4$  **3-Y** ( $17.7 \text{ cm}^3 \text{ K/mol}$ ) is in good agreement with the theoretical value for four non-interacting  $\text{Fe}^{\text{III}}$  ions ( $17.5 \text{ cm}^3 \text{ K/mol}$ ). On lowering the temperature, the  $\chi T$  product remains almost constant until 30 K, consistent with isolated  $\text{Fe}^{\text{III}}$  ions, but then rapidly decreases to reach  $12.0 \text{ cm}^3 \text{ K mol}^{-1}$  at 1.8 K (Figure 2). This decrease might in principle result from ZFS for the  $\text{Fe}^{\text{III}}$  ions, weak antiferromagnetic  $\text{Fe}-\text{Fe}$  interactions mediated via the diamagnetic  $\text{Y}^{\text{III}}$  ions, or a combination of these. Intermolecular interactions are highly unlikely, since the hydrogen bonding in **3-Y** is all intramolecular, and the only intermolecular interactions are between aliphatic  $\text{CH}_2$  groups and terminal nitrogens of the azide ligands, meaning there is no feasible pathway for intermolecular superexchange between  $\text{Fe}^{\text{III}}$  ions in different rings.

This is further qualitatively supported by the field dependence of the magnetization at low temperatures, in which the magnetization reaches  $19.9 \mu_B$  at 7 T (Figure 2). The magnitude of magnetization is in good agreement with the expected value ( $4 \times 5.0 \mu_B$ ) considering four isolated or very weakly antiferromagnetically coupled  $\text{Fe}^{\text{III}}$  ions. However, the reduced magnetization curves ( $M$  vs  $H/T$ ) measured at 2, 3, and 5 K do not superpose, indicating that weak  $\text{Fe}-\text{Fe}$  interactions result in low-lying excited states and/or that there is a significant single-ion anisotropy for the  $\text{Fe}^{\text{III}}$  ions (Figure S2, right).

Using Hamiltonian (1)

$$\hat{H} = -2J_{\text{FeFe}} \sum_{i=1}^4 \hat{s}_{\text{Fe},i} \cdot \hat{s}_{\text{Fe},i+1} + D_{\text{Fe}} \sum_{i=1}^4 (\vec{e}_{\text{Fe},i} \cdot \hat{s}_{\text{Fe},i})^2 + g\mu_B \vec{B} \cdot \sum_{i=1}^4 \hat{s}_{\text{Fe},i} \quad g = 2.0 \quad (1)$$

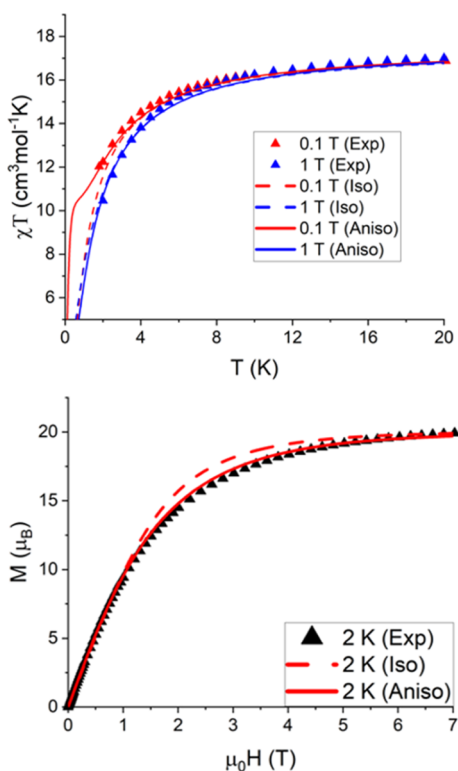


**Figure 2.** Magnetic susceptibility at  $B = 0.1$  T as well as  $B = 1.0$  T (top) and magnetization at  $T = 2$  K (bottom) of  $\text{Fe}_4\text{Y}_4$  (3-Y) highlighting the importance of the contribution of anisotropy to the fit. Both observables are obtained by exact diagonalization of Hamiltonian (1) and are evaluated using an angular (powder) average (see ref 23).

an excellent fit to the data (Figure 2) was obtained by the inclusion of single-ion anisotropy in a simultaneous fitting of both the susceptibility and magnetization data. This leads to a model with  $J_{\text{FeFe}} = -0.07$  K, in the same range as the calculated ones, and a single-ion iron easy axis anisotropy with  $D_{\text{Fe}} = -0.7$  K, which is also in the same order of magnitude as the calculated ones. The anisotropy is also the reason for the appearance of the knee-like shape for the  $\chi T$  curve at low field and temperature.

According to the fitting model the easy axis should be oriented in a plane with a relative angle of  $90^\circ$  between neighboring axes according to spin Hamiltonian (1) for  $\text{Fe}_4\text{Y}_4$ .<sup>24</sup>

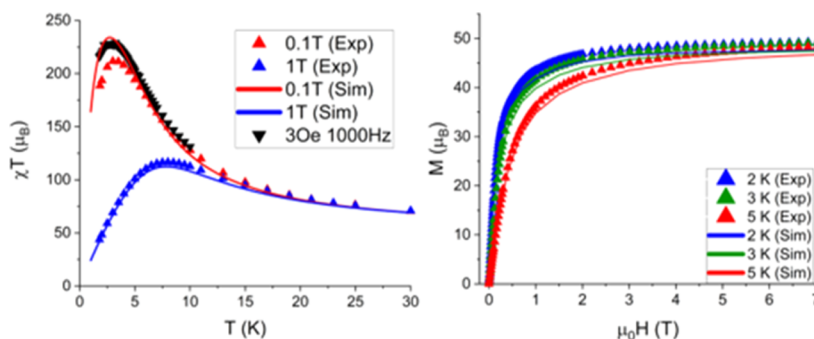


**Figure 3.** Magnetic susceptibility at  $B = 0.1$  T as well as  $B = 1.0$  T (left) and magnetization at  $T = 2, 3, 5$  K of  $\text{Fe}_4\text{Gd}_4$  (2-Gd) (right). Both observables are evaluated using an angular (powder) average (see ref 23).

Density functional theory (DFT) calculations (Siesta code and PBE functional, see the Supporting Information) confirmed the weak antiferromagnetic nature of the  $\text{Fe}\cdots\text{Fe}$  interactions, with  $J$  values in the range between  $-0.03$  and  $-0.12$  K (Table S3). In order to obtain additional information on the orientation of the magnetic anisotropy axes, we carried out CASSCF/NEVPT2 calculations with the Orca code using molecular models, see the Supporting Information.<sup>25</sup> The results (Figure S12) are consistent with the results of the fitting for three out of the four axes, confirming that the axial anisotropies of the  $\text{Fe}^{\text{III}}$  ions are the dominant contribution.

We now consider the magnetic properties of the  $\text{Fe}_4\text{Gd}_4$  ring 2-Gd, assuming that  $J_{\text{FeFe}}$  and  $D_{\text{Fe}}$  will have similar values to those found for 3-Y.

The  $\chi_M T$  value for 2-Gd at 300 K,  $48.78 \text{ cm}^3 \text{ K mol}^{-1}$ , is close to the theoretical value for four non-interacting high spin  $\text{Fe}^{\text{III}}$  ions and four  $\text{Gd}^{\text{III}}$  ions ( $49 \text{ cm}^3 \text{ K mol}^{-1}$  for  $g = 2.00$ ). As the temperature decreases,  $\chi_M T$  increases slowly but steadily, with this increase becoming steeper below 50 K. Under an applied field of 0.1 T, a maximum value of  $211.67 \text{ cm}^3 \text{ K mol}^{-1}$  is reached at 3.3 K, followed by a small but sharp decrease to reach  $188.15 \text{ cm}^3 \text{ K mol}^{-1}$  at 1.8 K (Figure 3 left). Using an AC applied field of 3 Oe at 1000 Hz to avoid saturation effects, the maximum value of  $\chi T$  is now higher, at  $228 \text{ cm}^3 \text{ K mol}^{-1}$ , but the downturn at low temperature, although smaller, is still present (Figure 3). Since the Fe–Fe interactions are expected to be antiferromagnetic, as found for 3-Y, such behavior indicates that ferromagnetic Fe–Gd interactions are dominant within the ring.

The field dependence of the magnetization curves at low temperatures shows a rapid increase at low fields with saturation at  $49.0 \mu_B$  at 7 T at 2 K (Figure 3 right), in agreement with a maximal spin  $S = 24$  and consistent with a fully ferromagnetic arrangement of the spins. However, the situation is not quite so simple.

The observed maximum  $\chi T$  value of  $228 \text{ cm}^3 \text{ K mol}^{-1}$  under the 3 Oe ac applied field seems to suggest a ground state with  $S = 21$ , rather than  $S = 24$ , although on close examination of the curve it turns out that, in the absence of the downturn,  $\chi_M T$  would extrapolate at low temperatures to ca.  $300 \text{ cm}^3 \text{ K mol}^{-1}$ , the theoretical value for  $S = 24$ , and  $g = 2.00$ . Furthermore, although the reduced magnetization curves at 2, 3, and 5 K superpose very cleanly, they cannot be reproduced by a simple Brillouin function for  $S = 24$ , although the curves lie closer to this function than they do to a sum of four  $S = 5/2$  and four  $S = 7/2$  Brillouin functions (Figure S2, left). One possibility would be the presence of low-lying spin states with  $S < 24$ ,

close in energy to the ferromagnetic ground state, resulting from competition between the ferromagnetic Fe–Gd and weaker antiferromagnetic Fe–Fe interactions, comparable in magnitude to those found in the Fe<sub>4</sub>Y<sub>4</sub> ring. Such competition was also seen in the Fe<sub>10</sub>Gd<sub>10</sub> ring.<sup>5</sup> The final decrease in  $\chi T$  below 3 K is likely to result, at least in part, from the ZFS of the Fe<sup>III</sup> ions, since the latter will have a similar  $D_{\text{Fe}}$  (−0.7 K) to those in the Fe<sub>4</sub>Y<sub>4</sub> ring 3-Y.

As for 3-Y, DFT calculations were also carried out on Fe<sub>4</sub>Gd<sub>4</sub> 2-Gd (see details in the Supporting Information).<sup>26,27</sup> These yield eight ferromagnetic  $J_{\text{FeGd}}$  coupling constants in the range +2.1 to +3.0 K, together with long-range  $J_{\text{FeFe}}$  couplings of +0.01 to −0.1 K and very weak ( $|J| < 0.04$  K) couplings between the Gd<sup>III</sup> ions (Table S5). Using these coupling constants, the experimental susceptibility curves were simulated using the PHI package (Figure S4).<sup>28</sup> However, the predicted increase in  $\chi_M T$  starts at higher temperatures, indicating that the calculated ferromagnetic  $J$  values are too high. The addition of the antiferromagnetic Fe–Fe coupling reproduced the low-temperature downturns in  $\chi_M T$  under the 0.1 and 1 T applied DC fields but could not model the downturn seen under the 3 Oe AC field, with the simulated curve extrapolating close to the theoretical value of 300 cm<sup>3</sup> K mol<sup>−1</sup> for  $S = 24$ .

In contrast to the Fe<sub>4</sub>Y<sub>4</sub> ring, exact diagonalization is no longer possible for the Fe<sub>4</sub>Gd<sub>4</sub> analogue. We therefore employed the finite-temperature Lanczos method<sup>29–31</sup> that yields excellent results for Heisenberg systems and very good results for anisotropic systems under sufficiently large applied magnetic fields. Unfortunately, this method typically leads to some intrinsic inaccuracies for fields as low as 0.1 T.

$$\begin{aligned} \hat{H} = & -2J_{\text{FeFe}} \sum_{i=1}^4 \hat{s}_{\text{Fe},i} \cdot \hat{s}_{\text{Fe},i+1} \\ & - 2J_{\text{FeGd}} \sum_{i=1}^4 (\hat{s}_{\text{Fe},i} \cdot \hat{s}_{\text{Gd},i} + \hat{s}_{\text{Fe},i} \cdot \hat{s}_{\text{Gd},i+1}) + D_{\text{Fe}} \sum_{i=1}^4 (\vec{e}_i \cdot \hat{s}_{\text{Fe},i})^2 \\ & + D_{\text{Gd}} \sum_{i=1}^4 (\vec{e}_{\text{Gd},i} \cdot \hat{s}_{\text{Gd},i})^2 + g\mu_B \vec{B} \cdot \sum_{i=1}^4 (\hat{s}_{\text{Fe},i} + \hat{s}_{\text{Gd},i}), \\ g = & 2.0 \end{aligned} \quad (2)$$

A fit of the magnetic data, see Figure 3, using the full Hamiltonian (2) for Fe<sub>4</sub>Gd<sub>4</sub> and assuming a powder average yields  $J_{\text{FeGd}} = +0.73$  K. If  $D_{\text{Fe}}$  has the same value as that found for the Fe<sub>4</sub>Y<sub>4</sub> ring, a single-ion anisotropy for the Gd<sup>III</sup> ions in Fe<sub>4</sub>Gd<sub>4</sub> is also required to reproduce the experimental data well. The available magnetic data are not sufficient to fix the absolute directions of the easy axis but only their relative orientations. However, assuming that all the anisotropy axes for the Fe as well as the Gd ions lie in the plane of the molecule and point radially outward gives a good fit and yields  $D_{\text{Gd}} = -0.7$  K. The  $D$  value of Gd<sup>III</sup> obtained from a fit to the magnetic data of Fe<sub>4</sub>Gd<sub>4</sub> is somewhat larger than previously reported values. We presume that it not only resembles single-ion anisotropy of Gd<sup>III</sup> but effectively also resembles other anisotropic terms not considered in the Hamiltonian (2) such as higher-order terms and dipolar as well as anisotropic exchange interactions.

CASSCF calculations were also performed in Gd model systems to evaluate the anisotropy. Analysis of the wavefunction reveals axial anisotropy with small energy differences

between states (Tables S6 and S7). The crystal field parameters with significant contributions are in all the cases  $B_2^0$  and  $B_2^2$ , with average values of −0.070 and 0.063 K, respectively (Table S8). This yields  $D = 3B_2^0 = -0.21$  K and  $E = B_2^2$ , corroborating the non-negligible axial anisotropy of Gd<sup>III</sup>.

In order to probe the magnetic behavior at very low temperatures, the magnetization of 2-Gd was also measured using an array of microSQUIDs (Figure 4). Interestingly, for a

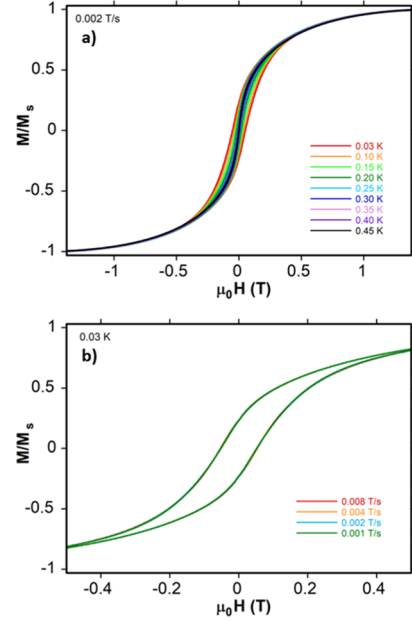


**Figure 4.** MicroSQUID hysteresis loop dependence with (a) temperature and (b) sweep rate at 30 mK for 2-Gd.

complex containing the supposedly isotropic Fe<sup>III</sup> and Gd<sup>III</sup> ions, weak hysteresis loops were observed below 0.3 K, with a coercive field of 106 mT at 30 mK. These saturate at 1.4 T (at which field the magnetization is known to have reached at least 48  $\mu_B$  at 2 K). These loops are temperature-dependent, but sweep-rate-independent (Figure 4).<sup>32,33</sup> If the relaxation data are plotted as an Arrhenius curve, a barrier to magnetization reversal of 9.4 K and a pre-exponential factor of  $10^{-13}$  s can be extracted (Figure S3, right). Although the latter corresponds to a higher rate than generally observed for typical SMMs, it is by no means exceptional, and may, e.g., result from the high density of excited states in 2-Gd. This is very likely related to the fact that the single-ion anisotropies are non-collinear. In view of the large ground-state spin of  $S = 24$  dipolar ordering might be possible as well at low temperatures.

The experimental entropy variation was obtained from the magnetization data using the Maxwell relation, i.e.,  $\Delta S(T)_{\Delta H} = \int [\partial M(T, H) / \partial T]_H dH$  (Figure 5). The maximum  $-\Delta S$  value at 7 T is 24.1 J kg<sup>−1</sup> K<sup>−1</sup> at 8 K. This temperature is significantly higher than values seen for other molecular systems, and certainly for Fe–Gd compounds, and the broad maximum over the temperature range 7–11 K is also noteworthy. The maximum  $-\Delta S_m$  value is about twice the value for a simple  $S = 24$  paramagnet (12.6 J kg<sup>−1</sup> T<sup>−1</sup>) but about half the value expected for non-interacting cations (50 J kg<sup>−1</sup> T<sup>−1</sup>), reflecting both the large number of low-lying excited magnetic states which contribute toward the overall entropy of the system and

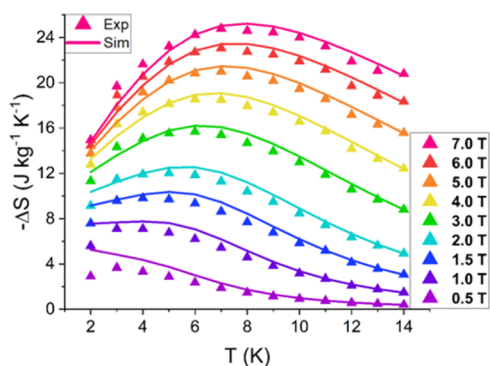


**Figure 5.** Isothermal magnetic entropy change of 2-Gd. Triangles show experimental data and solid lines show simulated data.

the weak magnetic interactions between the ions in the ring that result in these excited states. However, the much larger ferromagnetically coupled  $\text{Fe}_{10}\text{Gd}_{10}$  cyclic compound has  $\Delta S$  values more than four times larger than the values observed here.<sup>5</sup>

The theoretical magnetic entropy was evaluated using the parameters deduced from fitting the magnetization. The dependence of the isothermal entropy change both on temperature and field is very nicely reproduced. A comparison to calculations without anisotropy shows that then the slope at low  $T$  and  $B$  would not agree with the experimental data (see Figure S14). This is a second and independent strong hint that single-ion anisotropy cannot be neglected here.

## CONCLUSIONS

We have shown that  $\text{Fe}_4\text{Gd}_4$  is a magnetic cluster where the magnetic ions show rather strong single-ion anisotropy despite possessing a half-filled d- or f-shell, respectively. The commonly held belief that the more isotropic a system is the more likely it is to show a significant MCE, does not necessarily prove to be the case as was previously shown for systems containing  $\text{Fe}^{\text{III}}$  and  $\text{Gd}^{\text{III}}$ .<sup>5,22</sup> The thing that is different here is that both the “isotropic”  $\text{Fe}^{\text{III}}$  and  $\text{Gd}^{\text{III}}$  ions show appreciable single-ion anisotropy as evidenced from all magnetic observables, i.e. susceptibility, magnetization as well as isothermal entropy change. Moreover, the physical properties cannot be reproduced without assuming single-ion anisotropy in the Hamiltonian. We conjecture that the frustration due to competing interactions compresses the low-lying energy spectrum compared to non-frustrated systems which leads to a larger amount of entropy that can be swept by a magnetic field change.<sup>34</sup> In summary, we have a model that strongly suggests the necessity of single-ion anisotropy and that fits magnetic as well as MCE data rather well.

## AUTHOR INFORMATION

### Corresponding Authors

**Jürgen Schnack** – Fakultät für Physik, Universität Bielefeld, 33501 Bielefeld, Germany; Email: [jschnack@uni-bielefeld.de](mailto:jschnack@uni-bielefeld.de)

**Annie K. Powell** – Institute of Inorganic Chemistry (AOC), Karlsruhe Institute of Technology (KIT), 76131 Karlsruhe, Germany; Institute of Nanotechnology (INT), Karlsruhe Institute of Technology (KIT), 76344 Eggenstein-Leopoldshafen, Germany; Institute for Quantum Materials and Technologies (IQMT), Karlsruhe Institute of Technology (KIT), 76344 Eggenstein-Leopoldshafen, Germany; [orcid.org/0000-0003-3944-7427](https://orcid.org/0000-0003-3944-7427); Email: [annie.powell@kit.edu](mailto:annie.powell@kit.edu)

### Authors

**Dirk Schray** – Institute of Inorganic Chemistry (AOC), Karlsruhe Institute of Technology (KIT), 76131 Karlsruhe, Germany

**Dennis Westerbeck** – Fakultät für Physik, Universität Bielefeld, 33501 Bielefeld, Germany

**Jonas Braun** – Institute of Inorganic Chemistry (AOC), Karlsruhe Institute of Technology (KIT), 76131 Karlsruhe, Germany; Institute of Nanotechnology (INT), Karlsruhe Institute of Technology (KIT), 76344 Eggenstein-Leopoldshafen, Germany

**Yanhua Lan** – Institute of Inorganic Chemistry (AOC), Karlsruhe Institute of Technology (KIT), 76131 Karlsruhe, Germany

**Silvia Gómez-Coca** – Departament de Química Inorgànica and Institut de Recerca de Química Teòrica i Computacional, Universitat de Barcelona, 08028 Barcelona, Spain; [orcid.org/0000-0002-2299-4697](https://orcid.org/0000-0002-2299-4697)

**Wolfgang Wernsdorfer** – Institute of Nanotechnology (INT), Karlsruhe Institute of Technology (KIT), 76344 Eggenstein-Leopoldshafen, Germany; Physikalisches Institut (PHI), Karlsruhe Institute of Technology, 76131 Karlsruhe, Germany; Institute for Quantum Materials and Technologies (IQMT), Karlsruhe Institute of Technology (KIT), 76344 Eggenstein-Leopoldshafen, Germany; [orcid.org/0000-0003-4602-5257](https://orcid.org/0000-0003-4602-5257)

**Eliseo Ruiz** – Departament de Química Inorgànica and Institut de Recerca de Química Teòrica i Computacional, Universitat de Barcelona, 08028 Barcelona, Spain; [orcid.org/0000-0001-9097-8499](https://orcid.org/0000-0001-9097-8499)

**Christopher E. Anson** – Institute of Inorganic Chemistry (AOC), Karlsruhe Institute of Technology (KIT), 76131 Karlsruhe, Germany; [orcid.org/0000-0001-7992-7797](https://orcid.org/0000-0001-7992-7797)

### Auth or Contributions

D.S.: synthetic work; J.B., C.E.A., J.S., and A.K.P.: paper conceptualization and writing; Y.L.: magnetic SQUID measurements; W.W.: microSQUID measurements and interpretation; S.G.-C. and E.R.: DFT calculations; and D.W.

and J.S.: further theoretical treatment of magnetic and MCE data.

## Notes

The authors declare no competing financial interest.

## ACKNOWLEDGMENTS

All of this work was supported by funding from the DFG SFB/TR 88 "3MET". J.B. acknowledges the LGF for funding. E.R. and S.G.-C. thank the Spanish Ministerio de Ciencia e Innovación (PID2021-122464NB-I00 and Maria de Maeztu Excellence CEX2021-001202-M Grants) and Generalitat de Catalunya for an ICREA Academia award. The authors acknowledge computer resources, technical expertise, and assistance provided by the BSC.

## REFERENCES

- (1) Schray, D.; Abbas, G.; Lan, Y.; Mereacre, V.; Sundt, A.; Dreiser, J.; Waldmann, O.; Kostakis, G. E.; Anson, C. E.; Powell, A. K. Combined Magnetic Susceptibility Measurements and  $^{57}\text{Fe}$  Mössbauer Spectroscopy on a Ferro magnetic  $\{\text{Fe}(\text{III})_4\text{Dy}_4\}$  Ring. *Angew. Chem., Int. Ed.* **2010**, *49*, 5185–5188.
- (2) Baniodeh, A.; Hewitt, I. J.; Mereacre, V.; Lan, Y.; Novitchi, G.; Anson, C. E.; Powell, A. K. Heterometallic 20-membered  $\{\text{Fe}_{16}\text{Ln}_4\}$  (Ln = Sm, Eu, Gd, Tb, Dy, Ho) metallo-ring aggregates. *Dalton Trans.* **2011**, *40*, 4080–4086.
- (3) Baniodeh, A.; Liang, Y.; Anson, C. E.; Magnani, N.; Powell, A. K.; Unterreiner, A.-N.; Seyffler, S.; Slota, M.; Dressel, M.; Bogani, L.; Goß, K. Unraveling the Influence of Lanthanide Ions on Intra- and Inter-Molecular Electronic Processes in  $\text{Fe}_{10}\text{Ln}_{10}$  Nano-Toruses. *Adv. Funct. Mater.* **2014**, *24*, 6280–6290.
- (4) Botezat, O.; van Leusen, J.; Kravtsov, V. C.; Kögerler, P.; Baca, S. G. Ultralarge 3d/4f Coordination Wheels: From Carboxylate/Amino Alcohol-Supported  $\{\text{Fe}_4\text{Ln}_2\}$  to  $\{\text{Fe}_{18}\text{Ln}_6\}$  Rings. *Inorg. Chem.* **2017**, *56*, 1814–1822.
- (5) Baniodeh, A.; Magnani, N.; Lan, Y.; Buth, G.; Anson, C. E.; Richter, J.; Affronte, M.; Schnack, J.; Powell, A. K. High spin cycles: topping the spin record for a single molecule verging on quantum criticality. *npj Quantum Mater.* **2018**, *3*, 10.
- (6) Kaemmerer, H.; Baniodeh, A.; Peng, Y.; Moreno-Pineda, E.; Schulze, M.; Anson, C. E.; Wernsdorfer, W.; Schnack, J.; Powell, A. K. Inorganic Approach to Stabilizing Nanoscale Toroidicity in a Tetraicosanuclear  $\text{Fe}_{18}\text{Dy}_6$  Single Molecule Magnet. *J. Am. Chem. Soc.* **2020**, *142*, 14838–14842.
- (7) Baniodeh, A.; Anson, C. E.; Powell, A. K. Ringing the changes in  $\text{Fe}^{\text{III}}/\text{Yb}^{\text{III}}$  cyclic coordination clusters. *Chem. Sci.* **2013**, *4*, 4354–4361.
- (8) Cirera, J.; Ruiz, E.; Alvarez, S.; Neese, F.; Kortus, J. How to Build Molecules with Large Magnetic Anisotropy. *Chem.—Eur. J.* **2009**, *15*, 4078–4087.
- (9) Weighardt, K.; Pohl, K.; Jibril, I.; Huttner, G. Hydrolysis Products of the Monomeric Amine Complex  $(\text{C}_6\text{H}_{15}\text{N}_3)\text{FeCl}_3$ : The Structure of the Octameric Iron(III) Cation of  $\{[(\text{C}_6\text{H}_{15}\text{N}_3)\text{Fe}_8(\mu_3\text{-OH})_2(\mu_2\text{-OH})_{12}]\text{Br}_7(\text{H}_2\text{O})\}\text{Br}\cdot 8\text{H}_2\text{O}$ . *Angew. Chem., Int. Ed.* **1984**, *23*, 77–78.
- (10) Barra, A. L.; Debrunner, P.; Gatteschi, D.; Schulz, C. E.; Sessoli, R. Superparamagnetic-like behavior in an octanuclear iron cluster. *Europhys. Lett.* **1996**, *35*, 133–138.
- (11) Gatteschi, D.; Sorace, L.; Sessoli, R.; Barra, A. L. High Frequency EPR: an Occasion for Revisiting Ligand Field Theory. *Appl. Magn. Reson.* **2001**, *21*, 299–310.
- (12) Gatteschi, D.; Barra, A. L.; Caneschi, A.; Cornia, A.; Sessoli, R.; Sorace, L. EPR of molecular nanomagnets. *Coord. Chem. Rev.* **2006**, *250*, 1514–1529.
- (13) Holmberg, R. J.; Ho, L. T. A.; Ungur, L.; Korobkov, I.; Chibotaru, L. F.; Murugesu, M. Observation of unusual slow-relaxation of the magnetisation in a Gd-EDTA chelate. *Dalton Trans.* **2015**, *44*, 20321–20325.
- (14) Yoshida, T.; Cosquer, G.; Izuogu, D. C.; Ohtsu, H.; Kawano, M.; Lan, Y.; Wernsdorfer, W.; Nojiri, H.; Breedlove, B. K.; Yamashita, M. Field-Induced Slow Magnetic Relaxation of Gd(III) Complex with a Pt-Gd Heterometallic Bond. *Chem.—Eur. J.* **2017**, *23*, 4551–4556.
- (15) Chen, Y.-C.; Peng, Y.-Y.; Liu, J.-L.; Tong, M.-L. Field-induced slow magnetic relaxation in a mononuclear Gd(III) complex. *Inorg. Chem. Commun.* **2019**, *107*, 107449.
- (16) Handzlik, G.; Magott, M.; Arczynski, M.; Sheveleva, A. M.; Tuna, F.; Sarewicz, M.; Osyczka, A.; Rams, M.; Vieru, V.; Chibotaru, L. F.; Pinkowicz, D. Magnetization Dynamics and Coherent Spin Manipulation of a Propeller Gd(III) Complex with the Smallest Helicene Ligand. *J. Phys. Chem. Lett.* **2020**, *11*, 1508–1515.
- (17) Martínez-Pérez, M. J.; Cardona-Serra, S.; Schlegel, C.; Moro, F.; Alonso, P. J.; Prima-García, H.; Clemente-Juan, J. M.; Evangelisti, M.; Gaita-Arino, A.; Sese, J.; van Slageren, J.; Coronado, E.; Luis, F. Gd-based single-ion magnets with tunable magnetic anisotropy: molecular design of spin qubits. *Phys. Rev. Lett.* **2012**, *108*, 247213.
- (18) Senn, F.; Helm, L.; Borel, A.; Daul, C. A. Electronic fine structure calculation of  $[\text{Gd}(\text{DOTA})(\text{H}_2\text{O})]^-$  using LF-DFT: The zero field splitting. *C. R. Chim.* **2012**, *15*, 250–254.
- (19) Luis, F.; Alonso, P. J.; Roubeau, O.; Velasco, V.; Zueco, D.; Aguilà, D.; Martínez, J. I.; Barrios, L. A.; Aromi, G. A dissymmetric  $[\text{Gd}_2]$  coordination molecular dimer hosting six addressable spin qubits. *Commun. Chem.* **2020**, *3*, 176.
- (20) Clayton, J. A.; Keller, K.; Qi, M.; Wegner, J.; Koch, V.; Hintz, H.; Godt, A.; Han, S.; Jeschke, G.; Sherwin, M. S.; Yulikov, M. Quantitative analysis of zero-field splitting parameter distributions in Gd(III) complexes. *Phys. Chem. Chem. Phys.* **2018**, *20*, 10470–10492.
- (21) Glazkov, V. N.; Zhitomirsky, M. E.; Smirnov, A. I.; Krug von Nidda, H.-A.; Loidl, A.; Marin, C.; Sanchez, J.-P. Single-ion anisotropy in the gadolinium pyrochlores studied by electron paramagnetic resonance. *Phys. Rev. B: Condens. Matter Mater. Phys.* **2005**, *72*, 020409R.
- (22) Schmidt, S. F. M.; Koo, C.; Mereacre, V.; Park, J.; Heermann, D. W.; Kataev, V.; Anson, C. E.; Prodius, D.; Novitchi, G.; Klingeler, R.; Powell, A. K. A Three-Pronged Attack to Investigate the Electronic Structure of a Family of Ferromagnetic  $\text{Fe}_4\text{Ln}_2$  Cyclic Coordination Clusters: A Combined Magnetic Susceptibility, High-Field/High-Frequency Electron Paramagnetic Resonance, and  $^{57}\text{Fe}$  Mossbauer Study. *Inorg. Chem.* **2017**, *56*, 4796–4806.
- (23) Schnack, J. Magnetic response of magnetic molecules with non-collinear local d-tensors. *Condens. Matter Phys.* **2009**, *12*, 323–330.
- (24) Pister, D.; Irländer, K.; Westerbeck, D.; Schnack, J. Toroidal magnetic molecules stripped to their basics. *Phys. Rev. Res.* **2022**, *4*, 033221.
- (25) Neese, F. Software update: the ORCA program system, version 4.0. *Wiley Interdiscip. Rev.: Comput. Mol. Sci.* **2018**, *8*, No. e1327.
- (26) Perdew, J. P.; Burke, K.; Ernzerhof, M. Generalized Gradient Approximation Made Simple. *Phys. Rev. Lett.* **1996**, *77*, 3865–3868.
- (27) Soler, J. M.; Artacho, E.; Gale, J. D.; García, A.; Junquera, J.; Ordejón, P.; Sánchez-Portal, D. The SIESTA Method for ab initio order-N materials simulation. *J. Phys.: Condens. Matter* **2002**, *14*, 2745–2779.
- (28) Chilton, N. F.; Anderson, R. P.; Turner, L. D.; Soncini, A.; Murray, K. S. PHI: a powerful new program for the analysis of anisotropic monomeric and exchange-coupled polynuclear d- and f-block complexes. *J. Comput. Chem.* **2013**, *34*, 1164–1175.
- (29) Schnack, J.; Wendland, O. Properties of highly frustrated magnetic molecules studied by the finite-temperature Lanczos method. *Eur. Phys. J. B* **2010**, *78*, 535–541.
- (30) Hanebaum, O.; Schnack, J. Advanced finite-temperature Lanczos method for anisotropic spin systems. *Eur. Phys. J. B* **2014**, *87*, 194.
- (31) Schnack, J.; Richter, J.; Steinigeweg, R. Accuracy of the finite-temperature Lanczos method compared to simple typicality-based estimates. *Phys. Rev. Res.* **2020**, *2*, 013186.

(32) Liu, J.-L.; Chen, Y.-C.; Tong, M.-L. Symmetry strategies for high performance lanthanide-based single-molecule magnets. *Chem. Soc. Rev.* **2018**, *47*, 2431–2453.

(33) Boudalis, A. SMM-ET: An SMM Evaluation Tool for the Quantitative Treatment of Ac Susceptibility and Magnetic Hysteresis Data. *Quantum Mater. Res.* **2020**, *1*, No. e200004.

(34) Schnack, J. Large magnetic molecules and what we learn from them. *Contemp. Phys.* **2019**, *60*, 127–144.